

Supplementary Information

Mechanistic insights into electrocatalytic CO₂ reduction within [Ru^{II}(tpy)(NN)X]ⁿ⁺ architectures

Travis A. White, Somnath Maji, and Sascha Ott*

*Department of Chemistry, Ångström Laboratory, Uppsala Universitet
Box 523, 75120 Uppsala, Sweden. E-mail: sascha.ott@kemi.uu.se*

Table of Contents

Content	Page
Cover Page	S1
Table of Contents	S2
Figures S1-S3. $^1\text{H-NMR}$ spectra	S3-S4
Figure S4. Electronic absorption spectra	S5
Table S1. Electronic absorption data	S5
Figure S5. Simulated and experimental CVs	S6
Figures S6-S11. CVs of anodic and cathodic regions under argon	S7-S9
Figures S12-S15. CVs of scan rate variation throughout cathodic region	S10-S13
Figure S16. Gas chromatograms from bulk electrolysis experiment.	S14
Figures S17-S21. CVs of cathodic region under argon and CO_2	S15-S19

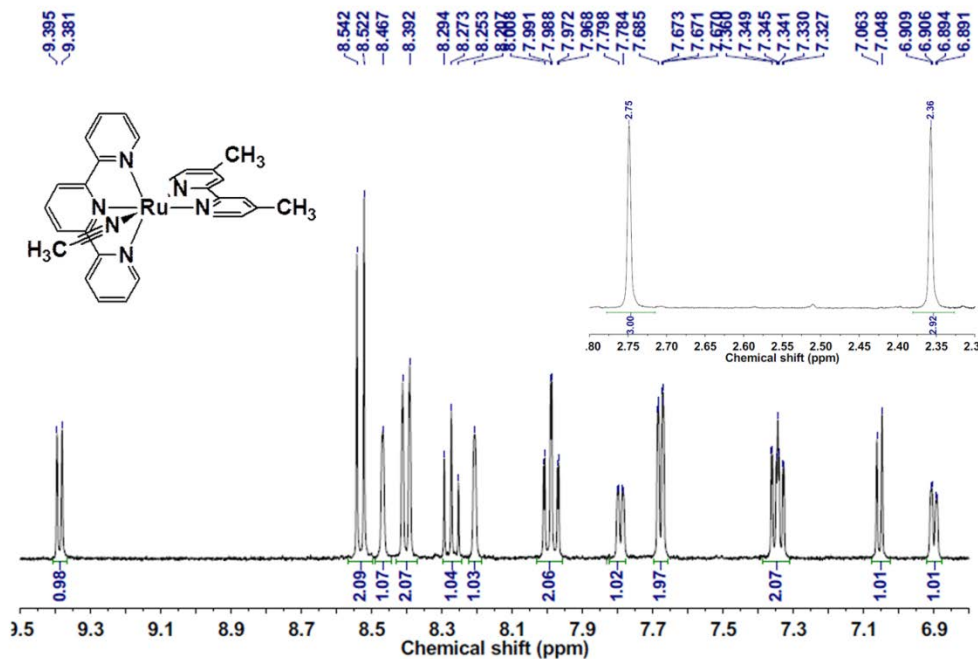


Figure S1. ^1H -NMR spectrum (400 MHz, CD_3CN) of $[\text{Ru}(\text{tpy})(4,4'\text{-Me}_2\text{bpy})\text{NCCH}_3](\text{PF}_6)_2$ at 25°C.

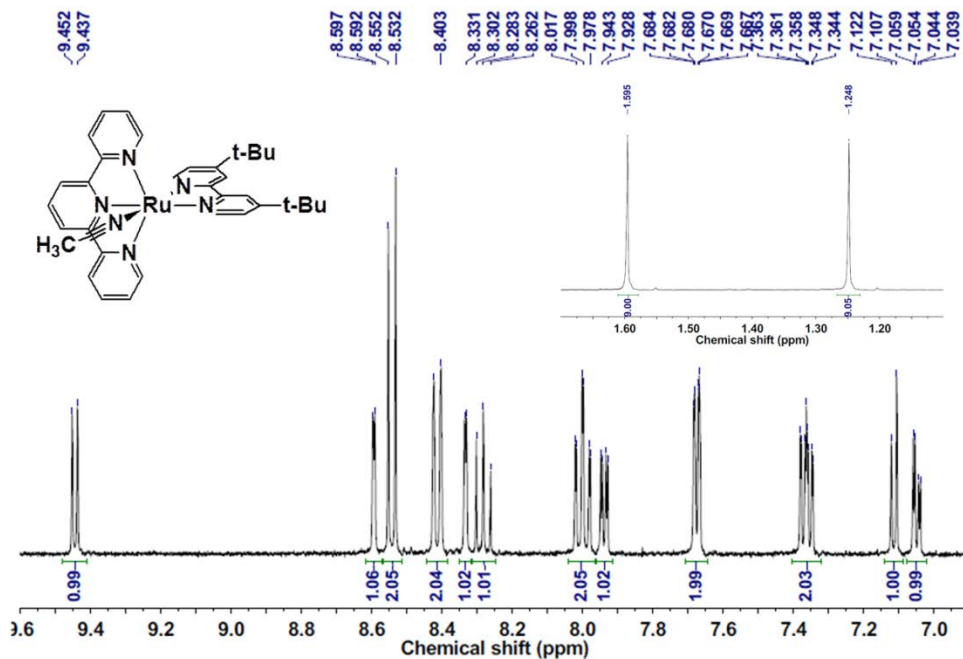


Figure S2. ^1H -NMR spectrum (400 MHz, CD_3CN) of $[\text{Ru}(\text{tpy})(4,4'\text{-}^4\text{Bu}_2\text{bpy})\text{NCCH}_3](\text{PF}_6)_2$ at 25°C.

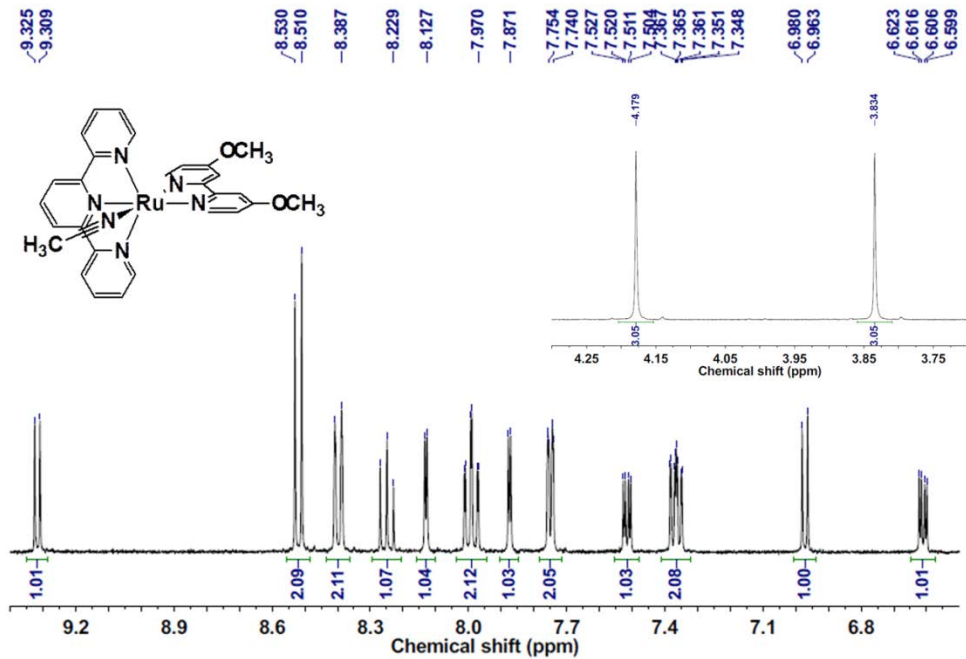


Figure S3. ^1H -NMR spectrum (400 MHz, CD_3CN) of $[\text{Ru}(\text{tpy})(\text{4},\text{4}'\text{-MeO})_2\text{bpy}]\text{NCCH}_3](\text{PF}_6)_2$ at 25°C.

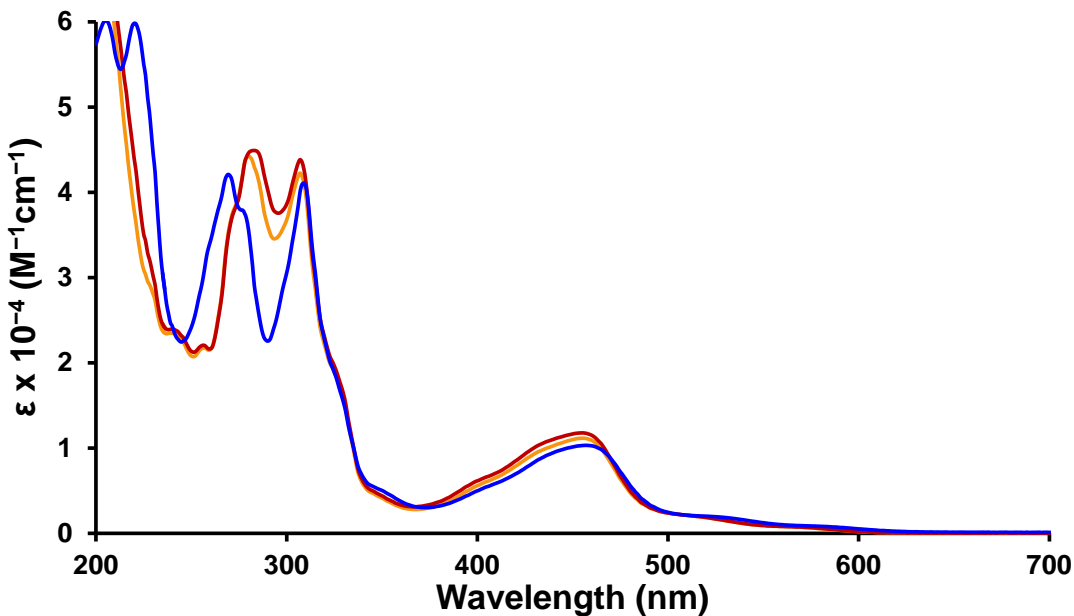


Figure S4. Electronic absorption spectra of $[\text{Ru}^{\text{II}}(\text{tpy})(4,4'\text{-Me}_2\text{bpy})\text{NCCH}_3]^{2+}$ (orange), $[\text{Ru}^{\text{II}}(\text{tpy})(4,4'\text{-tBu}_2\text{bpy})\text{NCCH}_3]^{2+}$ (red), and $[\text{Ru}(\text{tpy})((4,4'\text{-MeO})_2\text{bpy})\text{NCCH}_3]^{2+}$ (blue) measured at room temperature in CH_3CN .

Table S1. Electronic Absorption Data^a

Complex	λ_{abs} (nm)	$\epsilon \times 10^{-4} (\text{M}^{-1}\text{cm}^{-1})$
$[\text{Ru}^{\text{II}}(\text{tpy})(4,4'\text{-Me}_2\text{bpy})\text{NCCH}_3]^{2+}$	280	4.42
	307	4.23
	455	1.12
$[\text{Ru}^{\text{II}}(\text{tpy})(4,4'\text{-tBu}_2\text{bpy})\text{NCCH}_3]^{2+}$	283	4.49
	307	4.38
	455	1.18
$[\text{Ru}(\text{tpy})((4,4'\text{-MeO})_2\text{bpy})\text{NCCH}_3]^{2+}$	269	4.21
	309	4.11
	457	1.03

^a Measured in CH_3CN solution at room temperature.

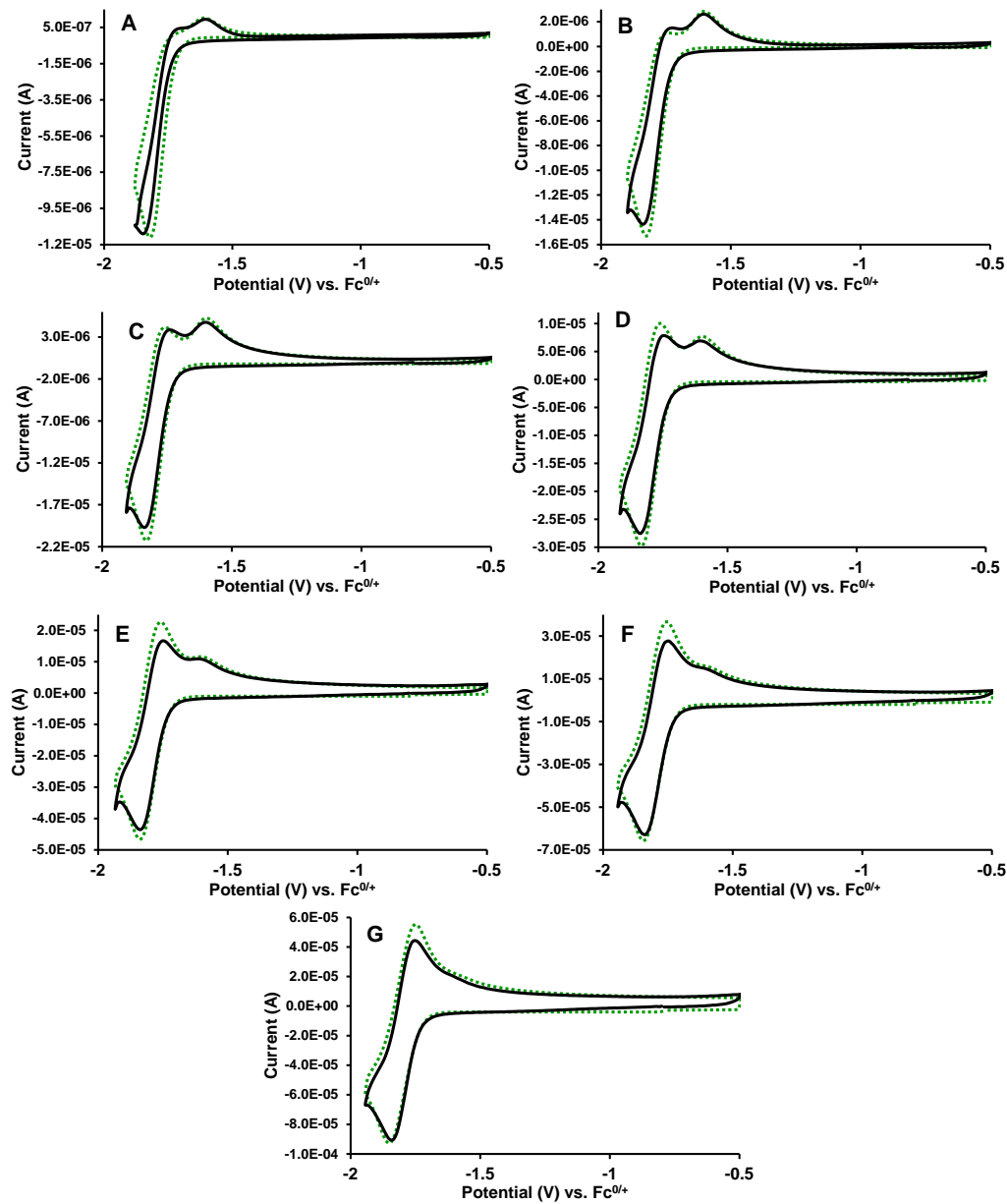


Figure S5. Experimental (solid black lines) and simulated (dotted green lines) cyclic voltammograms at 25 mV/s (**A**), 50 mV/s (**B**), 100 mV/s (**C**), 200 mV/s (**D**), 500 mV/s (**E**), 1000 mV/s (**F**), and 2000 mV/s (**G**) isolating the first redox couple upon cathodic scanning to calculate the rate constant for Cl^- dissociation ($k_{-\text{Cl}}$) for $[\text{Ru}^{\text{II}}(\text{tpy})(4,4'-(\text{MeO})_2\text{bpy})\text{Cl}]^+$. Parameters used to fit the simulated data to the experimental data were as follows: diffusion = Semi-Infinite 2D; geometry = disk; radius = 0.15 cm; $\alpha = 0.5$; $k_s = 10 \text{ cm/s}$; $E^0(\text{Ru}^{\text{III}/\text{I}}-\text{Cl}) = -1.73 \text{ V}$; $E^0(\text{Ru}^{\text{II}/\text{I}}-\text{NCCH}_3) = -1.53 \text{ V}$; $\text{Ru}^{\text{I}}-\text{Cl} \rightarrow \text{Ru}^{\text{I}}-\text{NCCH}_3 + \text{Cl}$ ($K_{\text{eq}} = 6.2$, $k_f = 0.6 \text{ s}^{-1}$, $k_b = 0.09677 \text{ s}^{-1}$); $\text{Ru}^{\text{I}}-\text{NCCH}_3 \rightarrow \text{Ru}^{\text{I}}$ ($K_{\text{eq}} = 329$, $k_f = 0.1452 \text{ s}^{-1}$, $k_b = 0.0004406 \text{ s}^{-1}$); $D(\text{Ru}^{\text{II}}-\text{Cl}) = 1.2 \times 10^{-5} \text{ cm}^2/\text{s}$; $D(\text{Ru}^{\text{I}}-\text{Cl}) = 6.6 \times 10^{-6} \text{ cm}^2/\text{s}$; $D(\text{Ru}^{\text{II}}-\text{NCCH}_3) = 8.5 \times 10^{-5} \text{ cm}^2/\text{s}$; $D(\text{Ru}^{\text{I}}-\text{NCCH}_3) = 7.6 \times 10^{-6} \text{ cm}^2/\text{s}$; $D(\text{Cl}) = 2.5 \times 10^{-6} \text{ cm}^2/\text{s}$; $D(\text{Ru}^{\text{I}}) = 1 \times 10^{-5} \text{ cm}^2/\text{s}$.

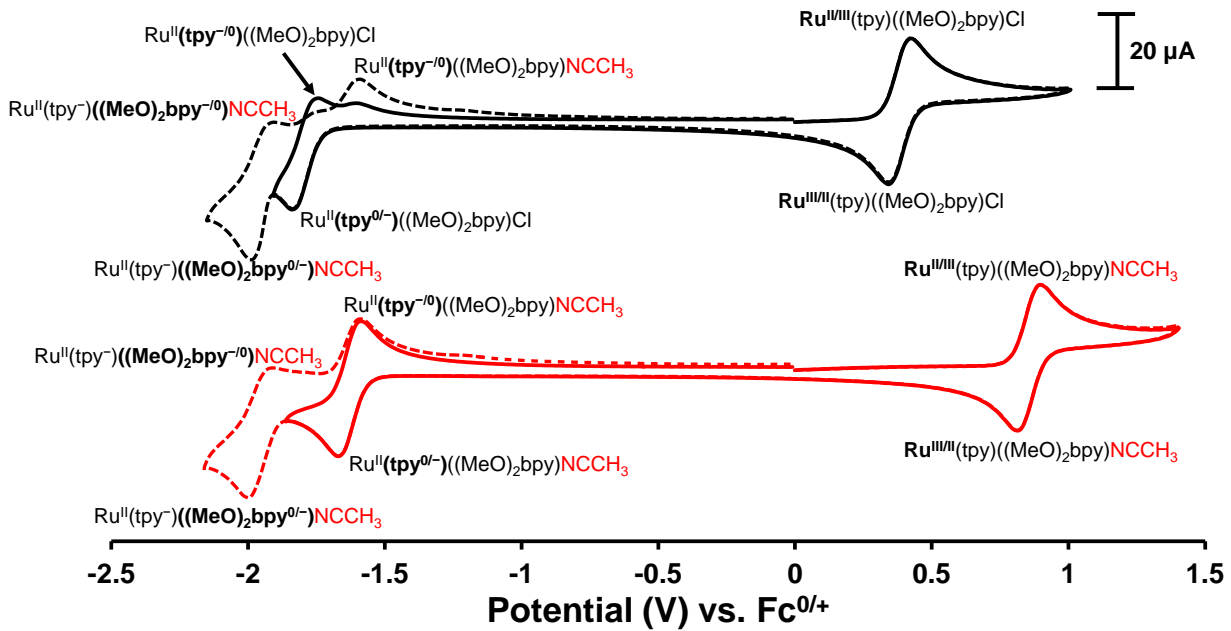


Figure S6. Cyclic voltammograms of $[\text{Ru}^{\text{II}}(\text{tpy})(4,4'-(\text{MeO})_2\text{bpy})\text{Cl}]^+$ (top) and $[\text{Ru}^{\text{II}}(\text{tpy})(4,4'-(\text{MeO})_2\text{bpy})\text{NCCH}_3]^{2+}$ (bottom) in Ar-saturated CH_3CN solution using 0.1 M Bu_4NPF_6 supporting electrolyte at $v = 200$ mV/s.

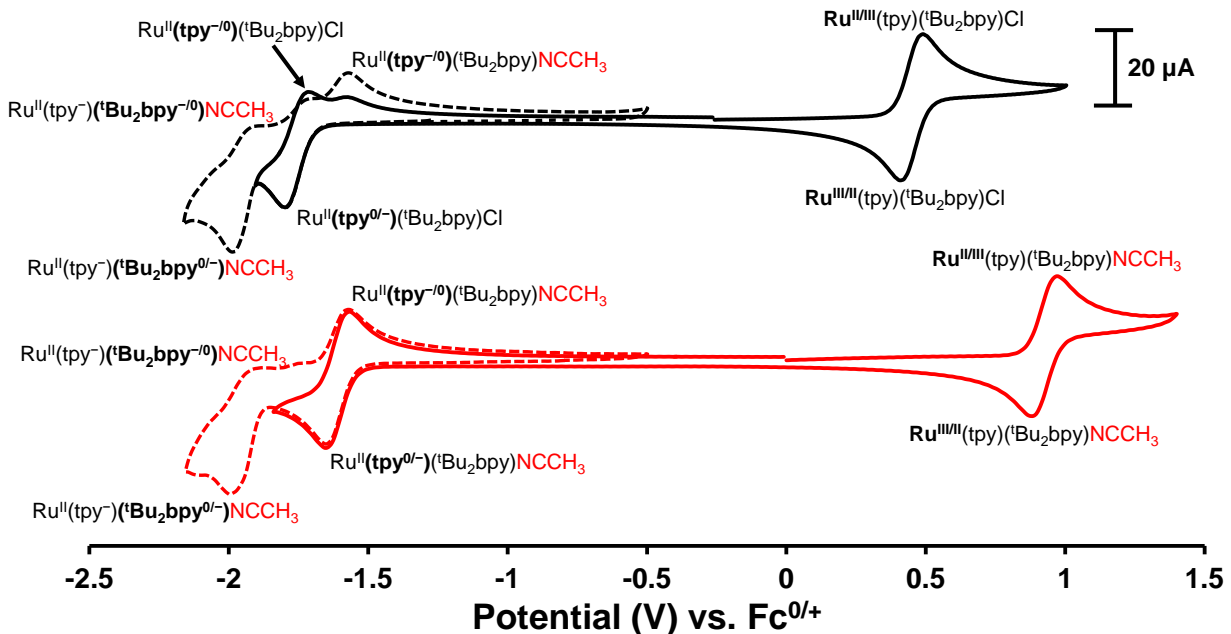


Figure S7. Cyclic voltammograms of $[\text{Ru}^{\text{II}}(\text{tpy})(4,4'-(\text{tBu}_2\text{bpy})\text{Cl}]^+$ (top) and $[\text{Ru}^{\text{II}}(\text{tpy})(4,4'-(\text{tBu}_2\text{bpy})\text{NCCH}_3]^{2+}$ (bottom) in Ar-saturated CH_3CN solution using 0.1 M Bu_4NPF_6 supporting electrolyte at $v = 200$ mV/s.

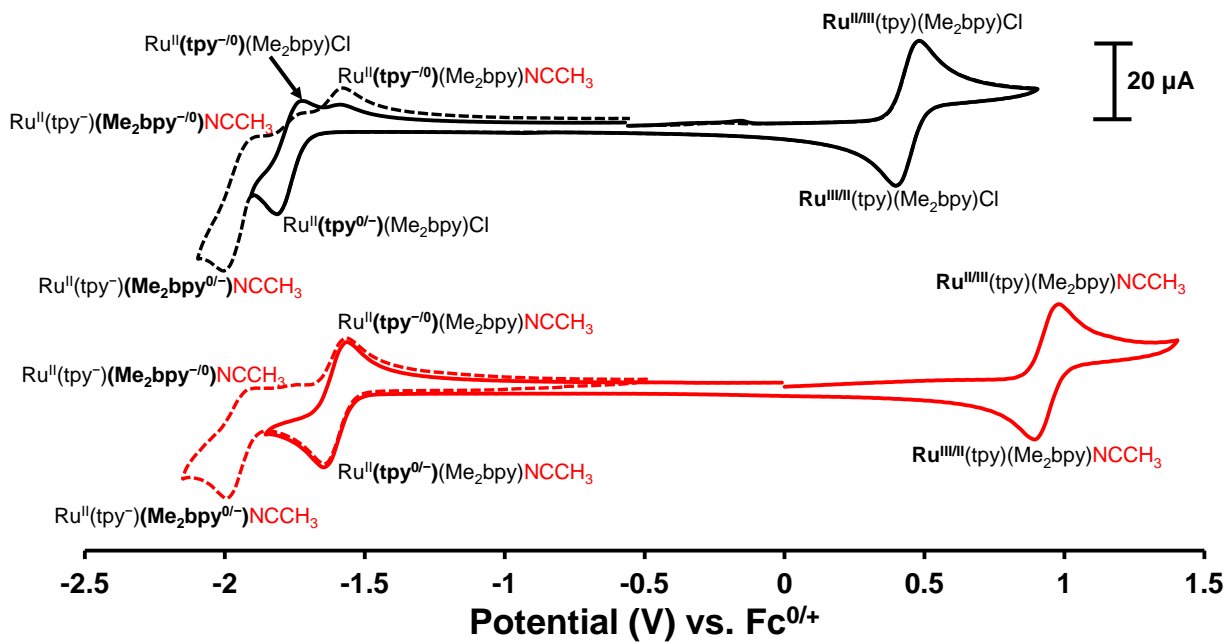


Figure S8. Cyclic voltammograms of [Ru^{II}(tpy)(4,4'-Me₂bpy)Cl]⁺ (top) and [Ru^{II}(tpy)(4,4'-Me₂bpy)NCCH₃]²⁺ (bottom) in Ar-saturated CH₃CN solution using 0.1 M Bu₄NPF₆ supporting electrolyte at v = 200 mV/s.

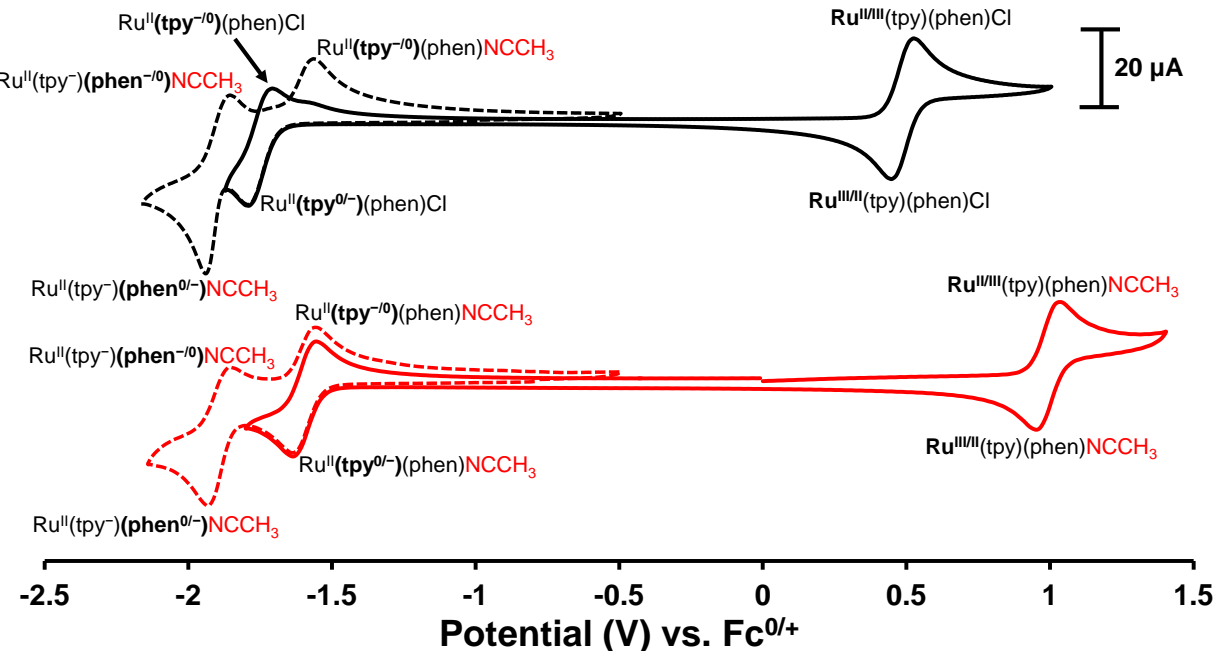


Figure S9. Cyclic voltammograms of [Ru^{II}(tpy)(phen)Cl]⁺ (top) and [Ru^{II}(tpy)(phen)NCCH₃]²⁺ (bottom) in Ar-saturated CH₃CN solution using 0.1 M Bu₄NPF₆ supporting electrolyte at v = 200 mV/s.

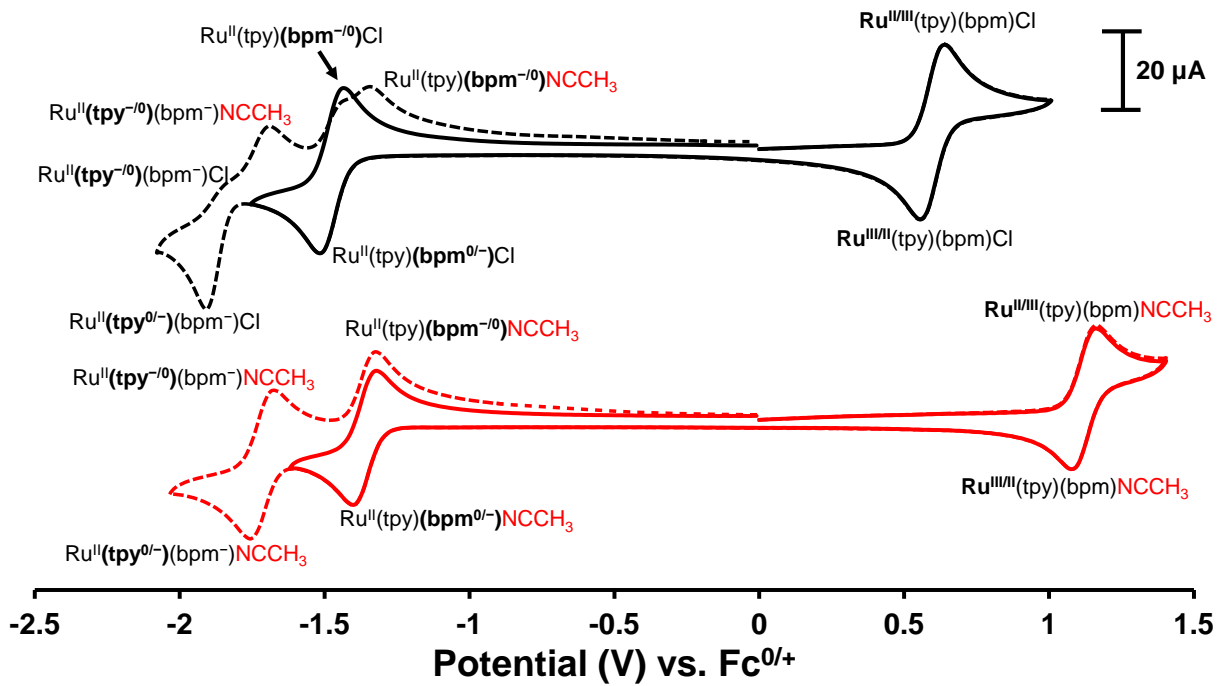


Figure S10. Cyclic voltammograms of $[\text{Ru}^{\text{II}}(\text{tpy})(\text{bpm})\text{Cl}]^+$ (top) and $[\text{Ru}^{\text{II}}(\text{tpy})(\text{bpm})\text{NCCH}_3]^{2+}$ (bottom) in Ar-saturated CH₃CN solution using 0.1 M Bu₄NPF₆ supporting electrolyte at $v = 200$ mV/s.

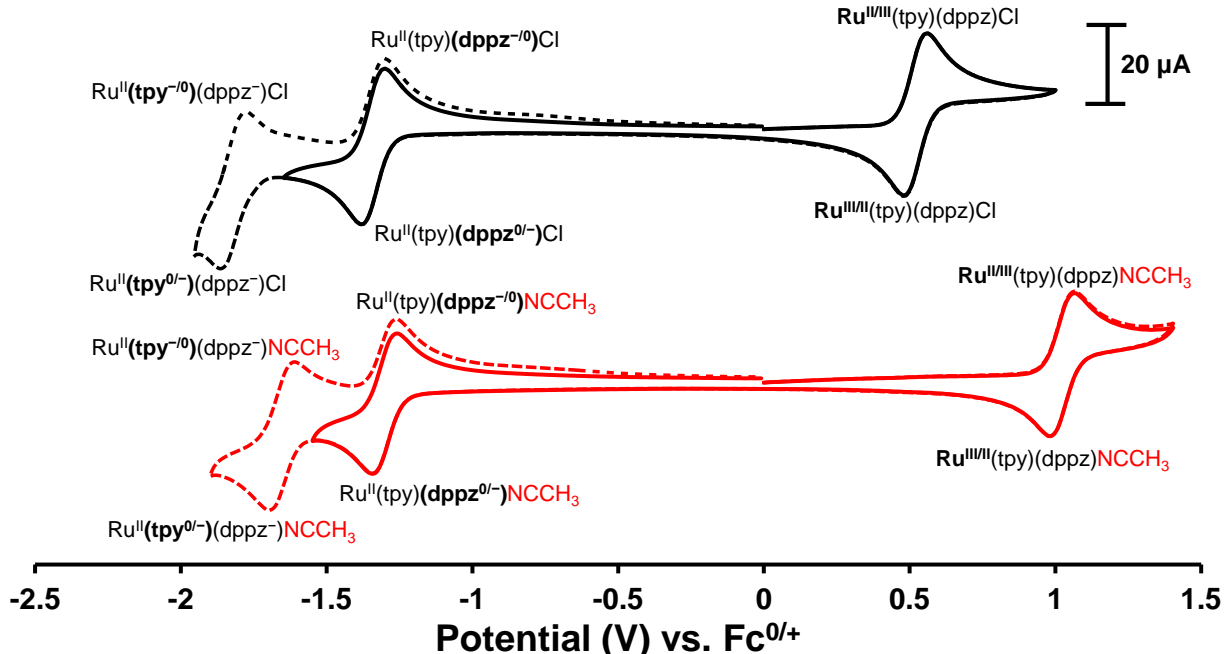


Figure S11. Cyclic voltammograms of $[\text{Ru}^{\text{II}}(\text{tpy})(\text{dppz})\text{Cl}]^+$ (top) and $[\text{Ru}^{\text{II}}(\text{tpy})(\text{dppz})\text{NCCH}_3]^{2+}$ (bottom) in Ar-saturated CH₃CN solution using 0.1 M Bu₄NPF₆ supporting electrolyte at $v = 200$ mV/s.

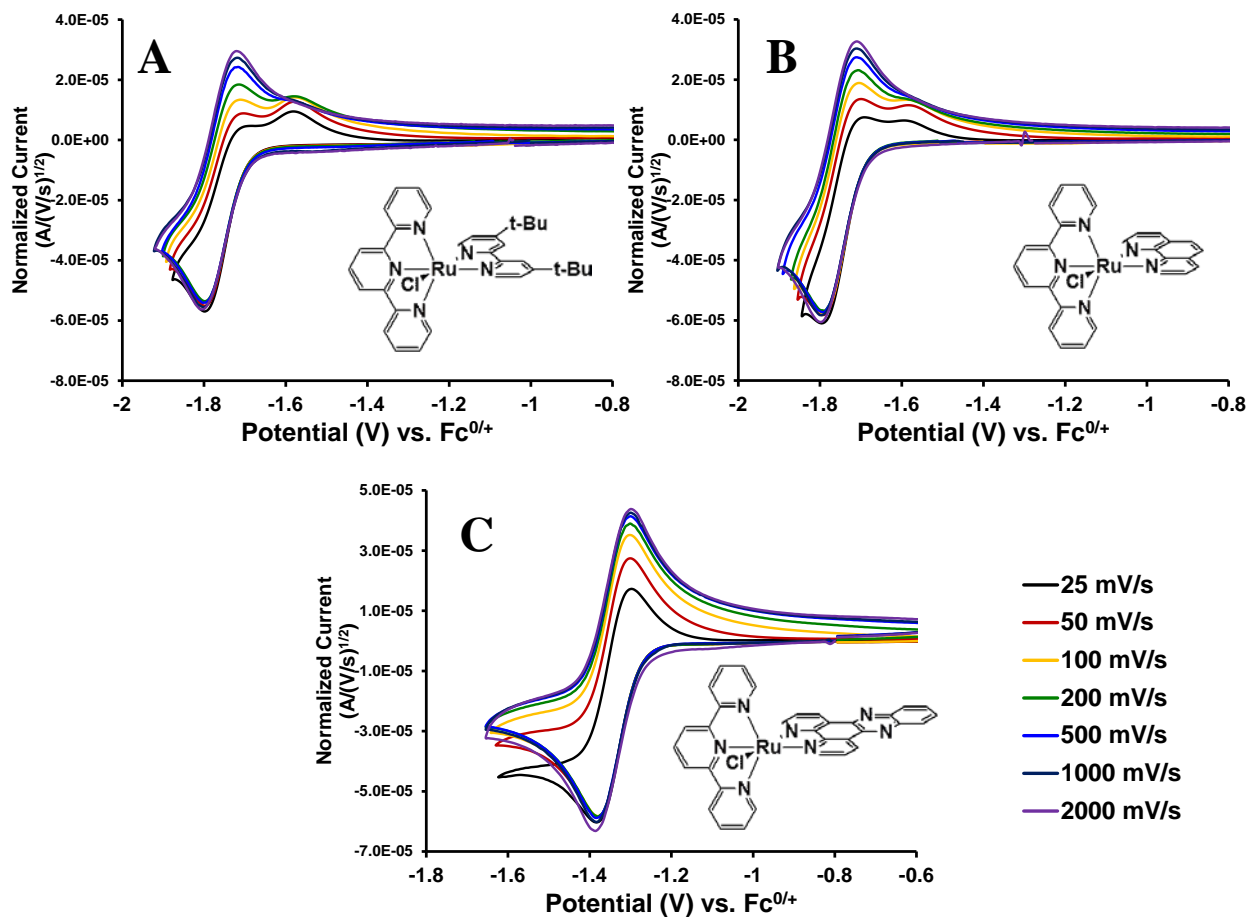


Figure S12. Scan rate variation of the 1st reduction within $[\text{Ru}^{\text{II}}(\text{tpy})(\text{tBu}_2\text{bpy})\text{Cl}]^+$ (**A**), $[\text{Ru}^{\text{II}}(\text{tpy})(\text{phen})\text{Cl}]^+$ (**B**), and $[\text{Ru}^{\text{II}}(\text{tpy})(\text{dppz})\text{Cl}]^+$ (**C**).

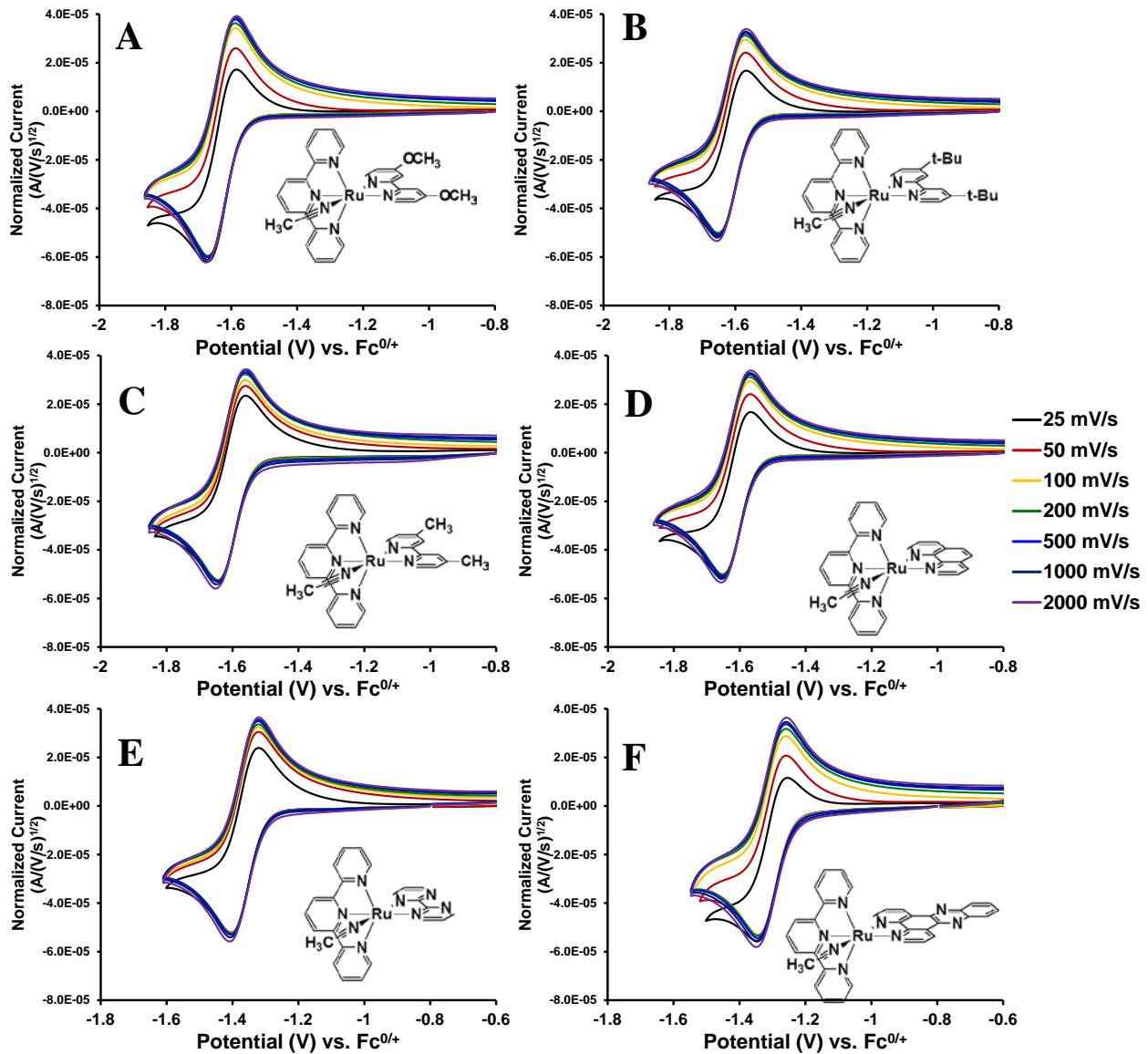


Figure S13. Scan rate variation of the 1st reduction within $[Ru^{II}(tpy)((MeO)_2bpy)NCCH_3]^{2+}$ (**A**), $[Ru^{II}(tpy)(^tBu_2bpy)NCCH_3]^{2+}$ (**B**), $[Ru^{II}(tpy)(Me_2bpy)NCCH_3]^{2+}$ (**C**), $[Ru^{II}(tpy)(phen)NCCH_3]^{2+}$ (**D**), $[Ru^{II}(tpy)(bpm)NCCH_3]^{2+}$ (**E**), and $[Ru^{II}(tpy)(dppz)NCCH_3]^{2+}$ (**F**).

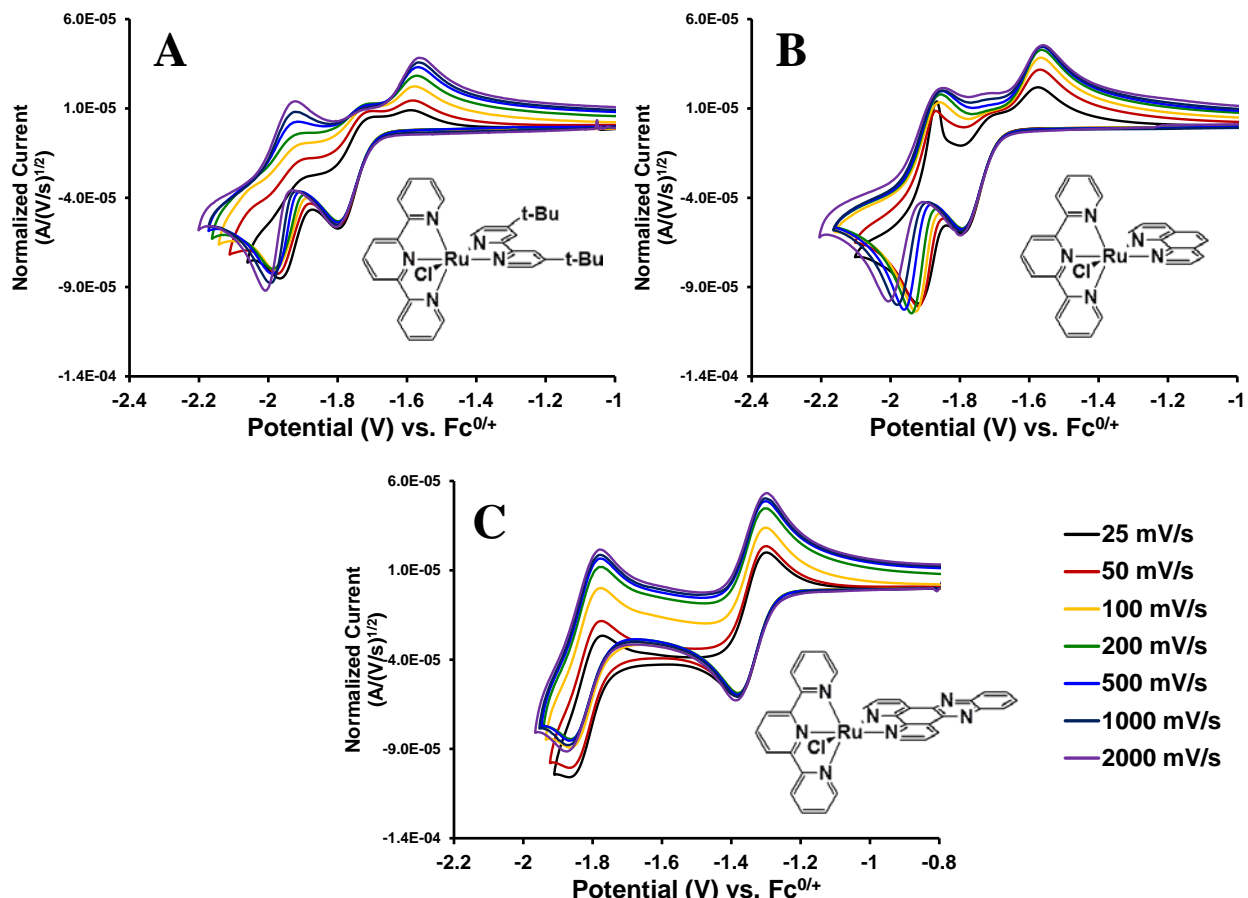


Figure S14. Scan rate variation of the 2nd reduction within $[Ru^{II}(tpy)(^tBu_2bpy)Cl]^+$ (**A**), $[Ru^{II}(tpy)(phen)Cl]^+$ (**B**), and $[Ru^{II}(tpy)(dppz)Cl]^+$ (**C**).

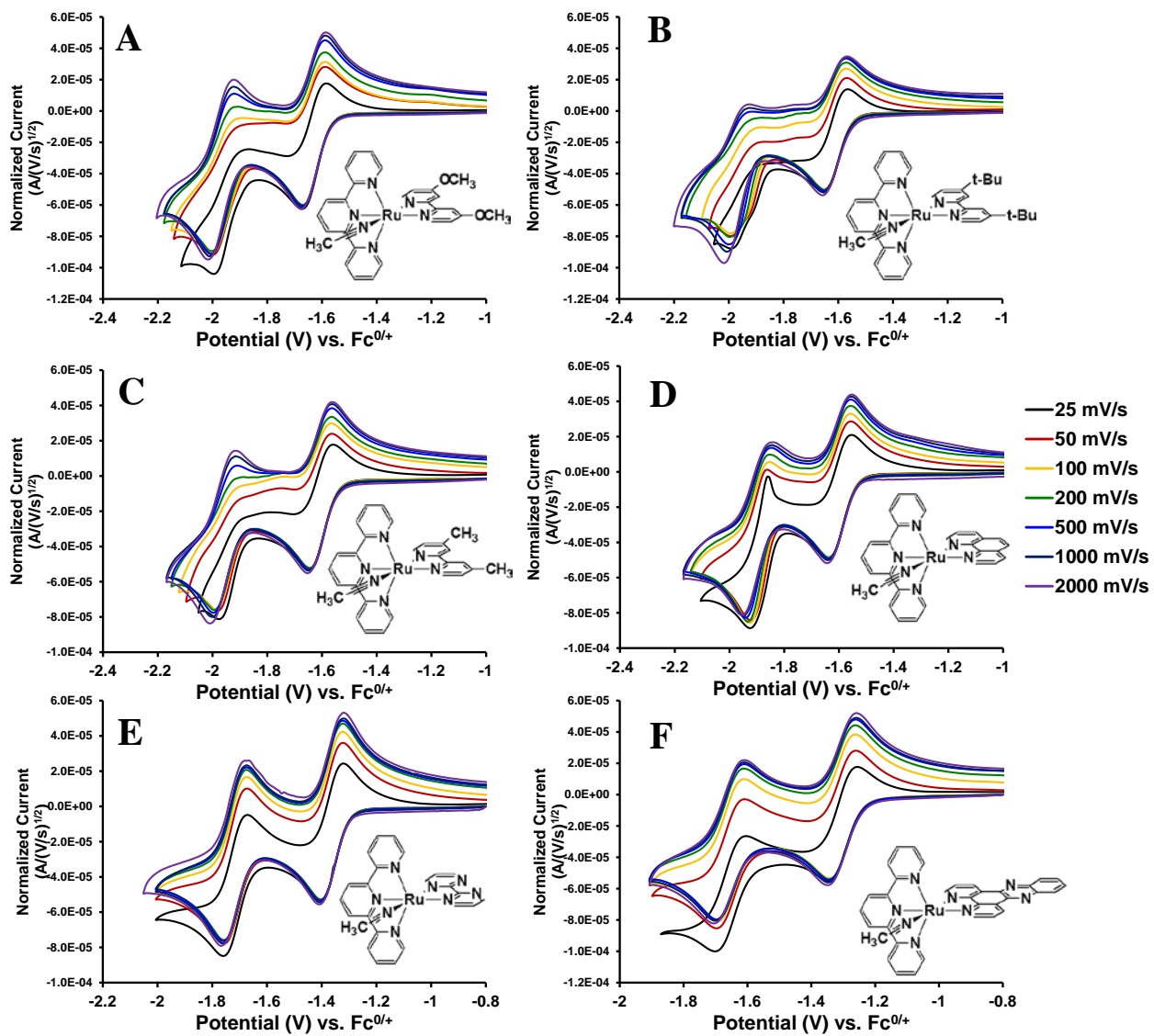


Figure S15. Scan rate variation of the 2nd reduction within $[Ru^{II}(tpy)((MeO)_2bpy)NCCH_3]^{2+}$ (A), $[Ru^{II}(tpy)(^tBu_2bpy)NCCH_3]^{2+}$ (B), $[Ru^{II}(tpy)(Me_2bpy)NCCH_3]^{2+}$ (C), $[Ru^{II}(tpy)(phen)NCCH_3]^{2+}$ (D), $[Ru^{II}(tpy)(bpm)NCCH_3]^{2+}$ (E), and $[Ru^{II}(tpy)(dppz)NCCH_3]^{2+}$ (F).

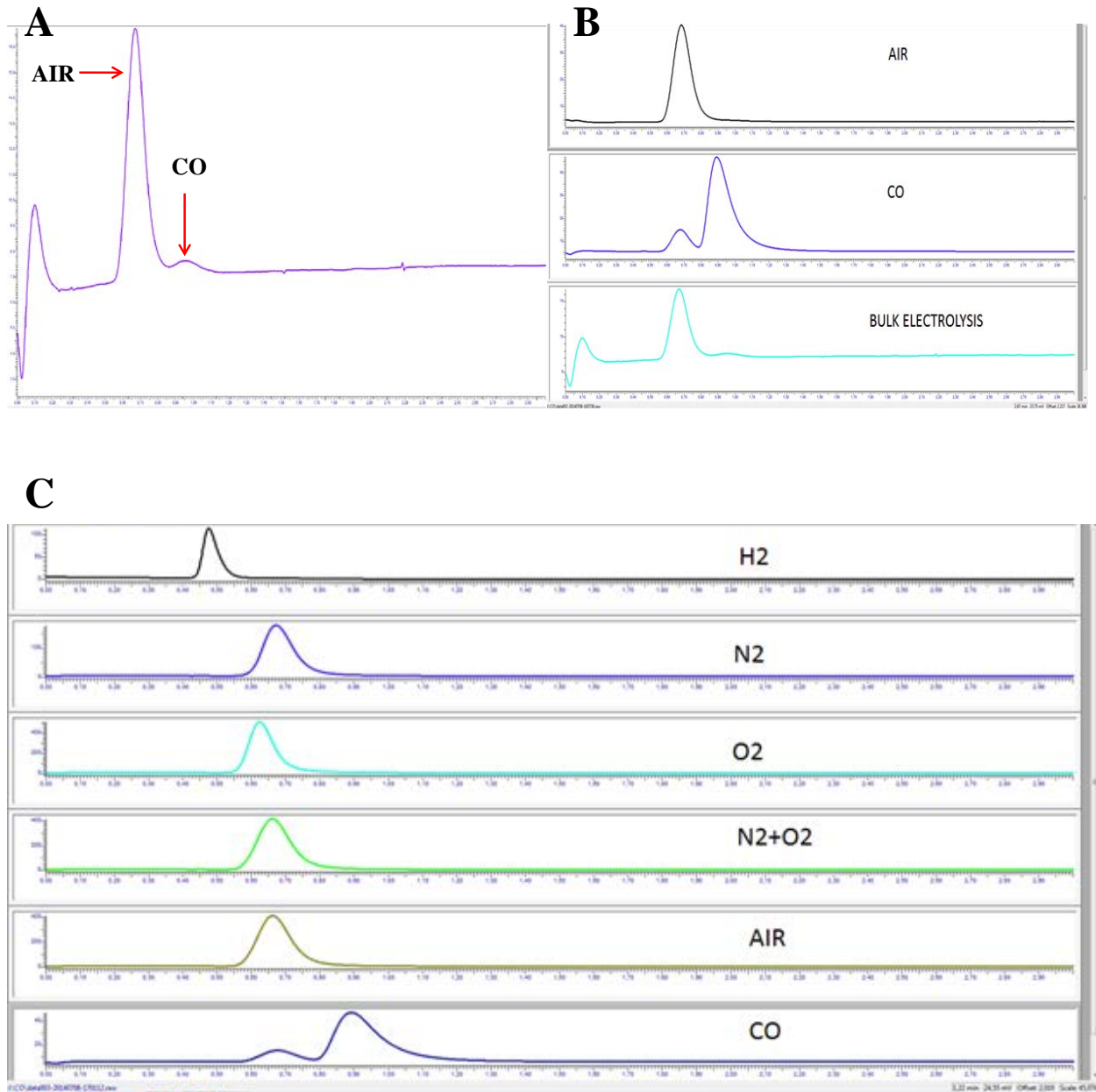


Figure S16. Gas chromatograms depicting a 250 μL injection of the headspace after 10 min bulk electrolysis of 1mM **1-CH₃CN** under a CO₂-saturated CH₃CN solution (**A**), comparison between injections of air, CO, and the bulk electrolysis products (**B**), and comparison between 50 μL injection of reference gas samples (**C**).

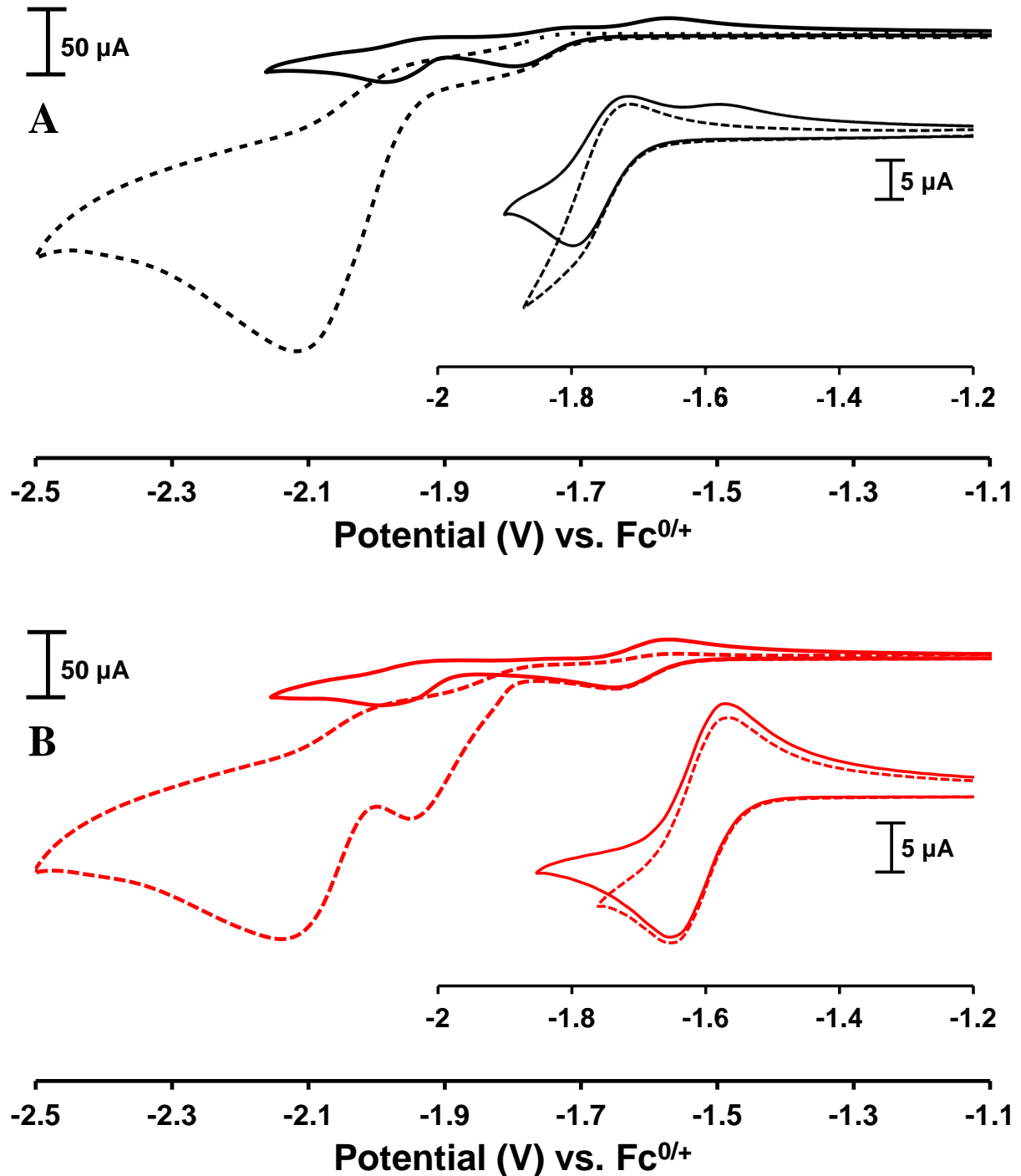


Figure S16. Cyclic voltammograms of $[\text{Ru}^{\text{II}}(\text{tpy})(4,4'\text{-tBu}_2\text{bpy})\text{Cl}]^+$ (**A**) and $[\text{Ru}^{\text{II}}(\text{tpy})(4,4'\text{-tBu}_2\text{bpy})\text{NCCH}_3]^{2+}$ (**B**) in Ar-saturated (solid line) and CO₂-saturated (dashed line) CH₃CN solutions using 0.1 M Bu₄NPF₆ supporting electrolyte at $v = 200$ mV/s. Inset: Isolation of 1st reduction process under Ar (solid) and CO₂ (dashed) atmospheres.

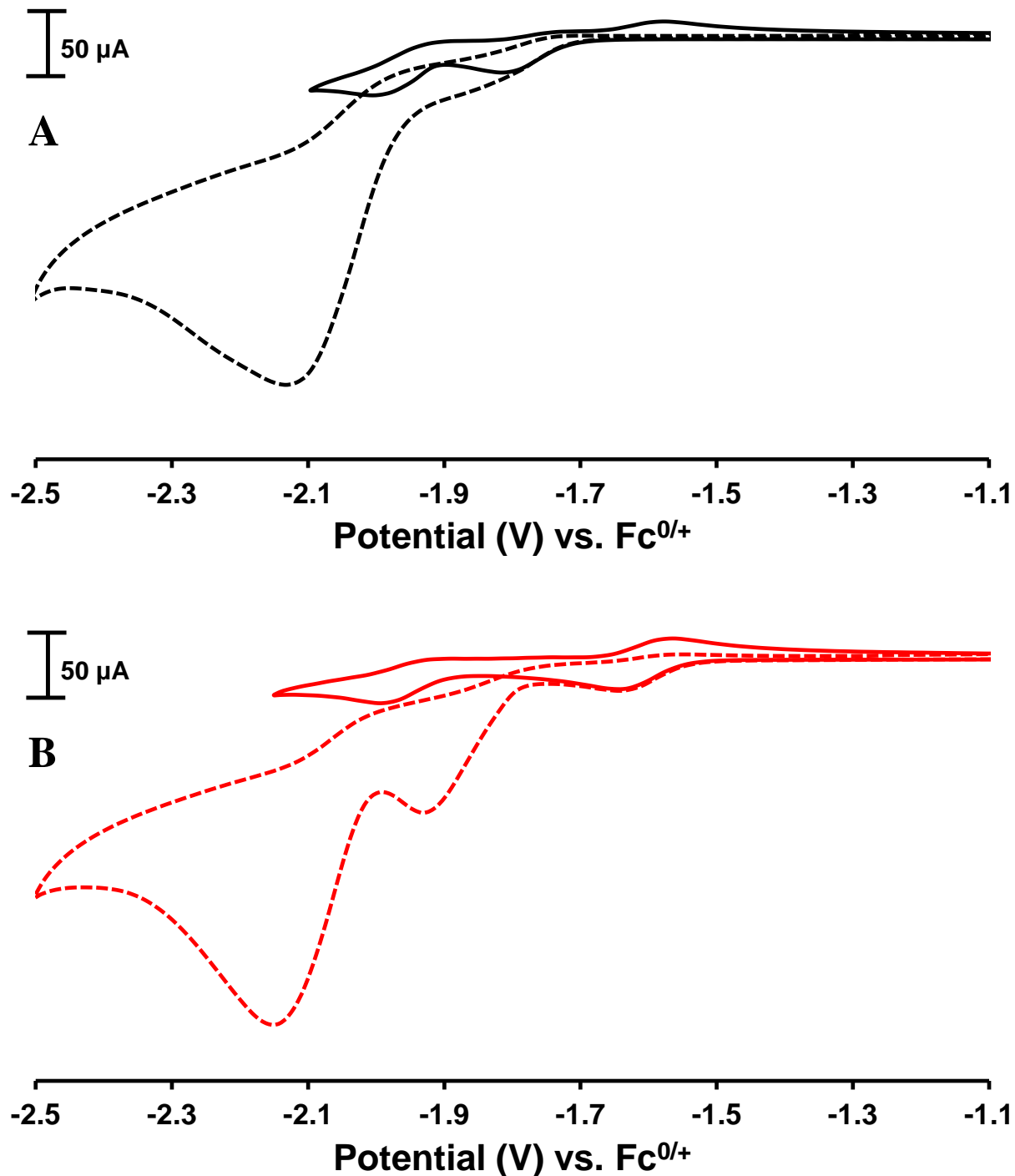


Figure S17. Cyclic voltammograms of $[\text{Ru}^{\text{II}}(\text{tpy})(4,4'\text{-Me}_2\text{bpy})\text{Cl}]^+$ **(A)** and $[\text{Ru}^{\text{II}}(\text{tpy})(4,4'\text{-Me}_2\text{bpy})\text{NCCH}_3]^{2+}$ **(B)** in Ar-saturated (solid line) and CO_2 -saturated (dashed line) CH_3CN solutions using 0.1 M Bu_4NPF_6 supporting electrolyte at $v = 200 \text{ mV/s}$.

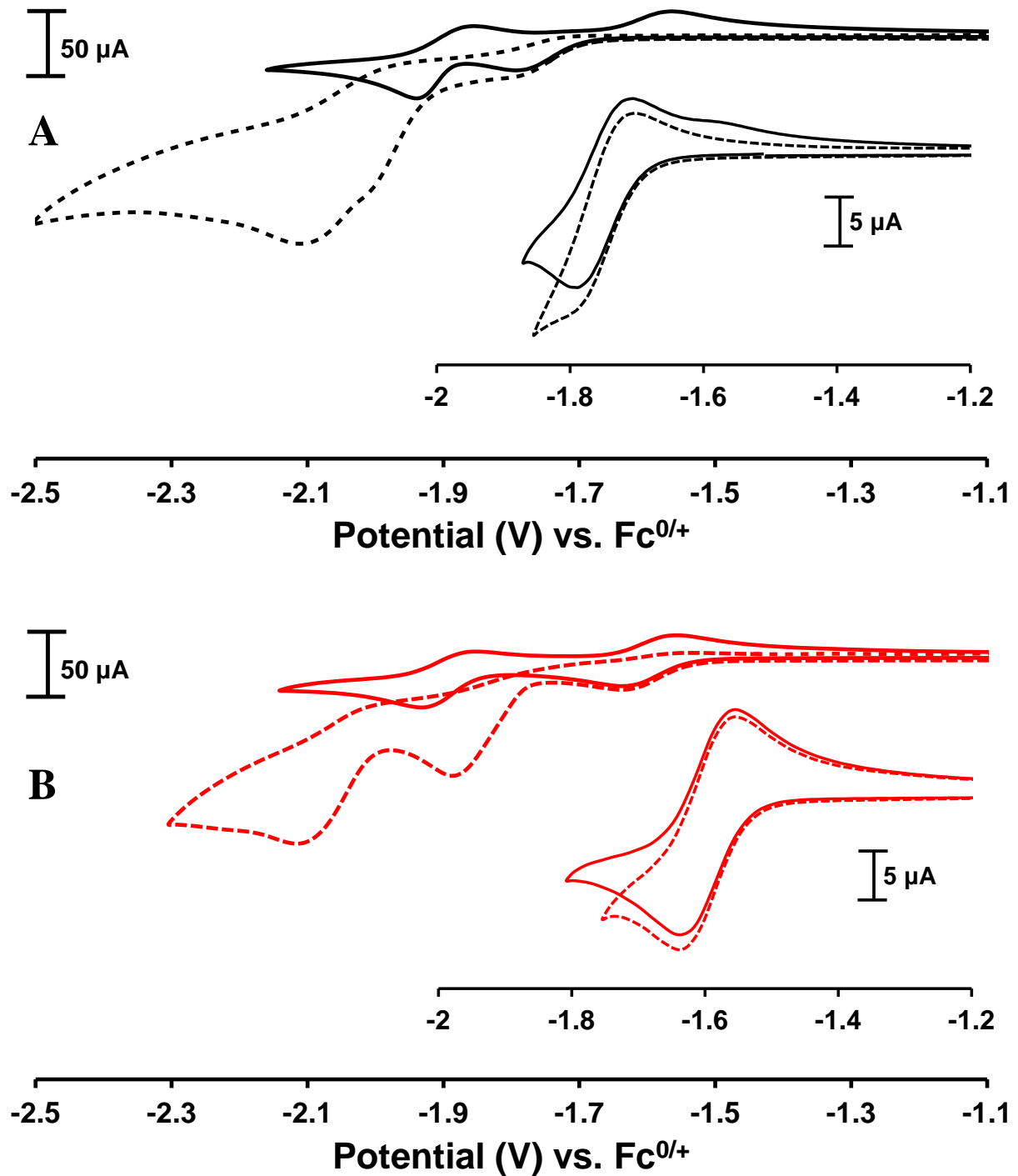


Figure S18. Cyclic voltammograms of $[\text{Ru}^{\text{II}}(\text{tpy})(\text{phen})\text{Cl}]^+$ (**A**) and $[\text{Ru}^{\text{II}}(\text{tpy})(\text{phen})\text{NCCH}_3]^{2+}$ (**B**) in Ar-saturated (solid line) and CO₂-saturated (dashed line) CH₃CN solutions using 0.1 M Bu₄NPF₆ supporting electrolyte at $v = 200$ mV/s. Inset: Isolation of 1st reduction process under Ar (solid) and CO₂ (dashed) atmospheres.

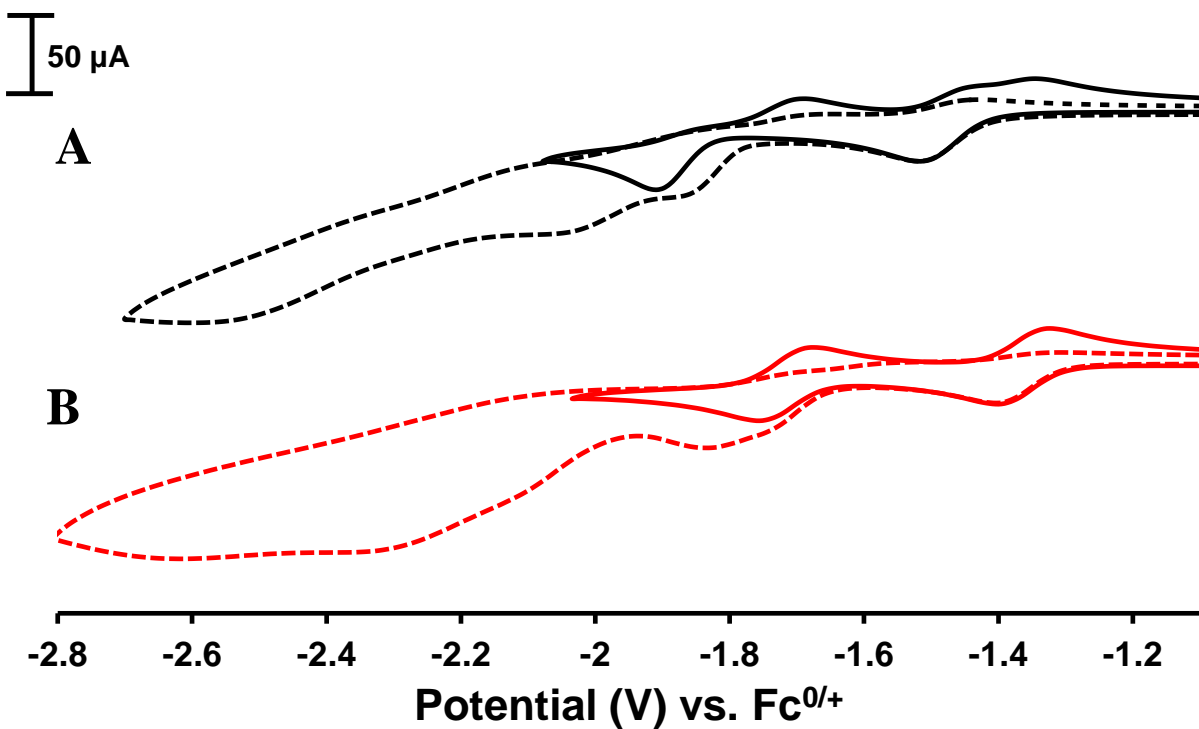


Figure S19. Cyclic voltammograms of $[\text{Ru}^{\text{II}}(\text{tpy})(\text{bpm})\text{Cl}]^+$ (**A**) and $[\text{Ru}^{\text{II}}(\text{tpy})(\text{bpm})\text{NCCH}_3]^{2+}$ (**B**) in Ar-saturated (solid line) and CO_2 -saturated (dashed line) CH_3CN solutions using 0.1 M Bu_4NPF_6 supporting electrolyte at $v = 200$ mV/s.

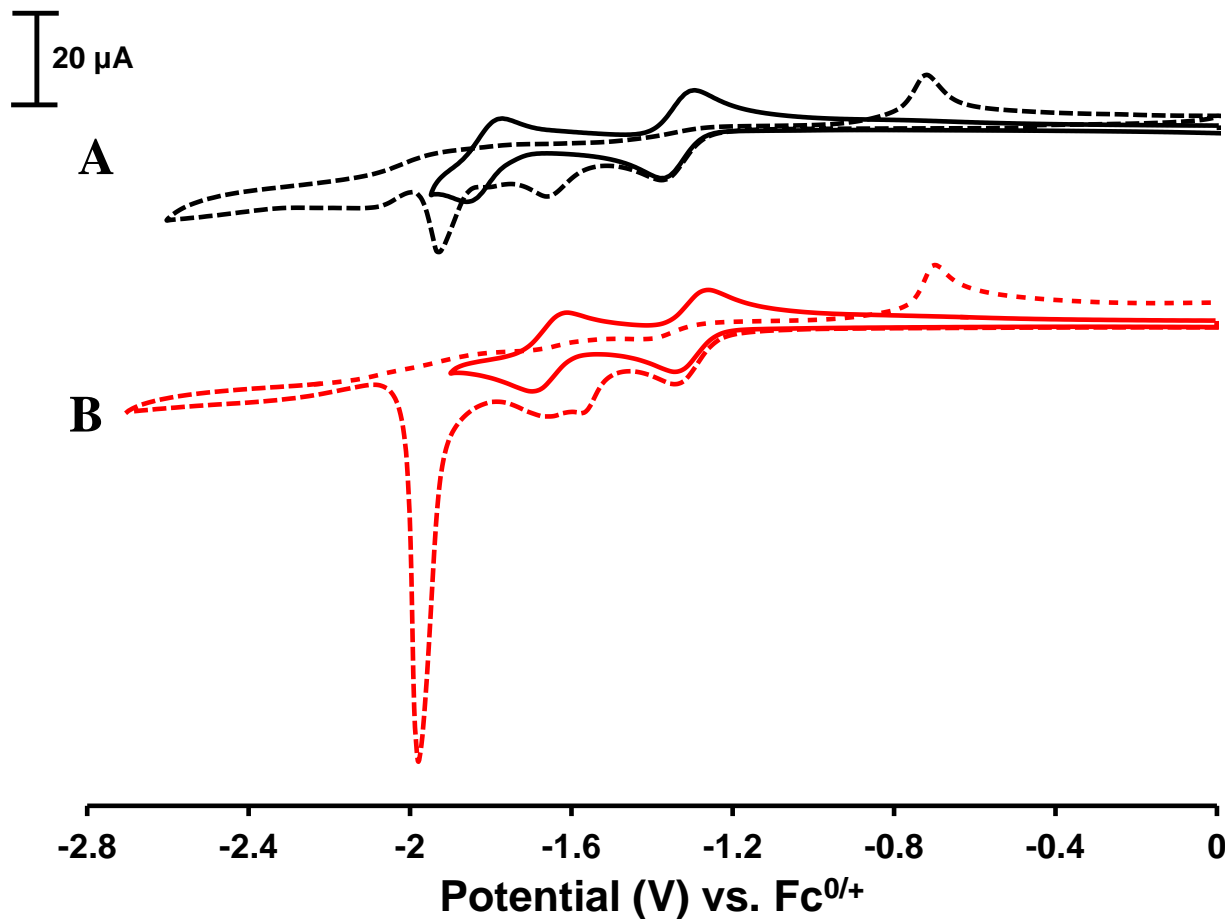


Figure S20. Cyclic voltammograms of $[\text{Ru}^{\text{II}}(\text{tpy})(\text{dppz})\text{Cl}]^+$ (**A**) and $[\text{Ru}^{\text{II}}(\text{tpy})(\text{dppz})\text{NCCH}_3]^{2+}$ (**B**) in Ar-saturated (solid line) and CO_2 -saturated (dashed line) CH_3CN solutions using 0.1 M Bu_4NPF_6 supporting electrolyte at $v = 200$ mV/s.